ARCHIVES OF ELECTRICAL ENGINEERING VOL. 63(1), pp. 47-61 (2014)

DOI 10.2478/aee-2014-0004

3D loss and heat analysis at the end region of 4-poles 1150 MW nuclear power turbine generator

GUANG-HOU ZHOU[1,2], LI HAN[1], ZHEN-NAN FAN[1], YONG LIAO[1], SONG HUANG[1]

[1] *State Key Laboratory of Power Transmission Equipment & System Safety and New Technology Chongqing University, Chongqing ,400030, P. R. China*

[2] *Dongfang Electrical Machinery Company Limited, Deyang, 618000, P. R. China*
e-mail: fanzhennan@ 126.com

(Received: 22.08.2013, revised: 29.10.2013)

Abstract: To study the principle of loss and heat at the end region of large 4-poles nuclear power turbine generator, 3D transient electromagnetic field and 3D steady temperature field finite element (FE) models of the end region are established respectively. Considering the factors such as rotor motion, core non-linearity and time-varying of electromagnetic field, the anisotropic heat conductivity and different heat dissipation conditions of stator end region, a 50 Hz, 1150 MW, 4-poles nuclear power turbine generator is investigated. The loss and heat at the generator end region are calculated respectively at no-load and rated-load, and the calculation results are compared with the test data. The result shows that the calculation model is accurate and the generator design is suitable. The method is valuable for the research of loss and heat at the end region of large 4-poles nuclear power turbine generator and the improvement of the generator's operation stability. The method has been applied successfully for the design of the larger nuclear power turbine generators.

Key words: loss and heat, end region, 4-poles nuclear power turbine generator, electromagnetic field, temperature field

1. Introduction

The eddy current loss caused by the magnetic field at the end region of a large turbine generator is the main reason of the end region heat. To prevent the overheat and ensure the safe operation of the generator and the power system, the loss and heat analysis at the end region should be researched in detail. Especially, the 3D numerical analysis of loss and heat at the end region of large 4-poles nuclear power turbine generators whose capacity is above 1000 MW is rarely mentioned in the public references. So the research about this issue is necessary.

However, for a long time, the researches about loss and heat calculation at the end region were focused on the 2-poles turbine generators. Due to the complex geometric structure and material characteristics at the end region of turbine generator, such as the magnetic shield, the clamping plate, the finger plate, the end ladder core, the end windings and so on, the 3D numerical analysis becomes quite difficult. The early researches usually adopted the 2D axis

symmetric models or quasi-3D models to solve the problems [1-4]. In [5], a general method for axiperiodic linear magnetostatic problems was developed to reduce the size of the electromagnetic field problem. In [6], a coupled method of quasi-3D field with circuit equations was presented to calculate the magnetic field of turbine generator end region. In [7], the boundary value problem and the variational problem of the eddy current electromagnetic field at the turbine generator end region were derived. And based on the simplified models of the specific structure, the end region magnetic field was calculated by 3D analytic method in [8]. The methods mentioned above are difficult to obtain the correct distribution of magnetic field and loss due to few considerations of the complete structure and the material characteristics. With the development of the magnetic field analysis and the improvement of computers, the 3D models were adopted in the magnetic field analysis at the end region of the turbine generators. The 3D static magnetic field models were adopted in [9, 10]. However, the time-varying and eddy current effects were not considered. The magnetic field and the eddy current were analyzed by the 3D steady AC magnetic field in [11], but the core saturation and the rotor motion were ignored, then the time-varying principle of eddy current loss was not obtained. The end region eddy current loss of different operation condition were analyzed by the 3D transient models in [12]. However, the heat problem were not involved.

In the aspect of heat calculation, in [4], the temperature distribution at the magnetic shield, the clamping plate and the end core were calculated by the 2D temperature field FE method. In [13, 14], the cylindrical coordinate and rectangular coordinate FE models were used to calculate the thermal distribution at the end region. In [15], the time-harmonic coupled field analysis was used to deal with the travelling electromagnetic field and the 3D temperature field for the end region of a 2-poles 1000 MW turbine generator. And in [16, 17], the temperature distribution at the end region were analyzed by the 3D fluid field. However the losses of these references were obtained by the quasi-3D magnetic field model or the 3D steady AC magnetic field model, and they may lead to the heat source inaccurate. And some references mentioned above did not consider the important components in the temperature field calculation, such as the magnetic shield, the finger plate and the end ladder core, so the accuracy of the results was not good [15]. For the 4-poles nuclear power turbine generators whose capacity is above 1000 MW, the 3D numerical analysis of loss and heat at the end region is rarely mentioned in the public references till now.

In this paper, a 50 Hz, 1150 MW, 4-poles nuclear power turbine generator operating at no-load and rated load is analyzed by 3D transient electromagnetic field, considering the factors such as the structure, the materials, the eddy current and the rotor motion. Then, the magnetic field loss distribution at the end region is obtained. Meanwhile, the 3D steady temperature model of the stator end region is built up and the temperature distribution of the end region is obtained.

2. Calculation models

2.1. Basic parameters of the generator

The basic parameters of the large 4-poles nuclear power turbine generator are listed in Table 1 and the generator structures is showed in Figure 1.

Table 1. The basic parameters of the generator

Parameter	Value
Rated power (MW)	1150
Rated voltage (kV)	24
Rated current (A)	30379
Rated power factor	0.9
Number of the magnetic poles	4
Number of the stator slots	48

a)

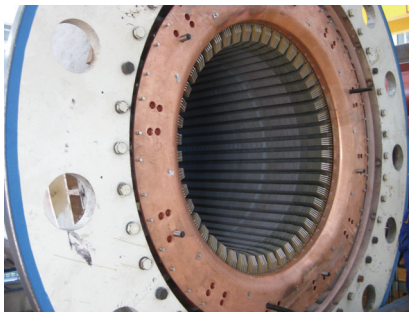

b)

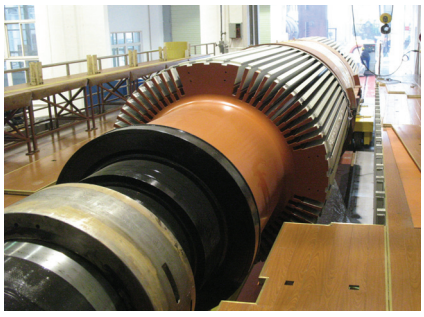

c)

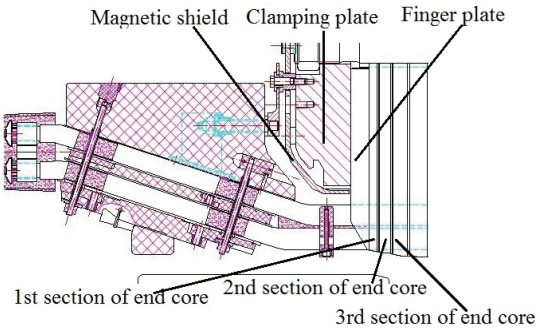

Fig. 1. Generator structures and the measure points of end region a): stator end region, b) rotor, c) structure of end region

According to the periodicity of the magnetic field, a quarter of the cylinder is chosen as the 3D electromagnetic field calculation region, as shown in Figure 2.

2.2. Boundary value problem of the 3D electromagnetic field

According to the practical engineering, the following assumptions are proposed.

1) The high-order harmonics of current in the windings and the impact of displacement current are ignored.
2) The stator and rotor cores are non-eddy current region.
3) The saturation effects of the stator and rotor cores are considered, their B-H curves are nonlinear, and their core materials are isotropic.

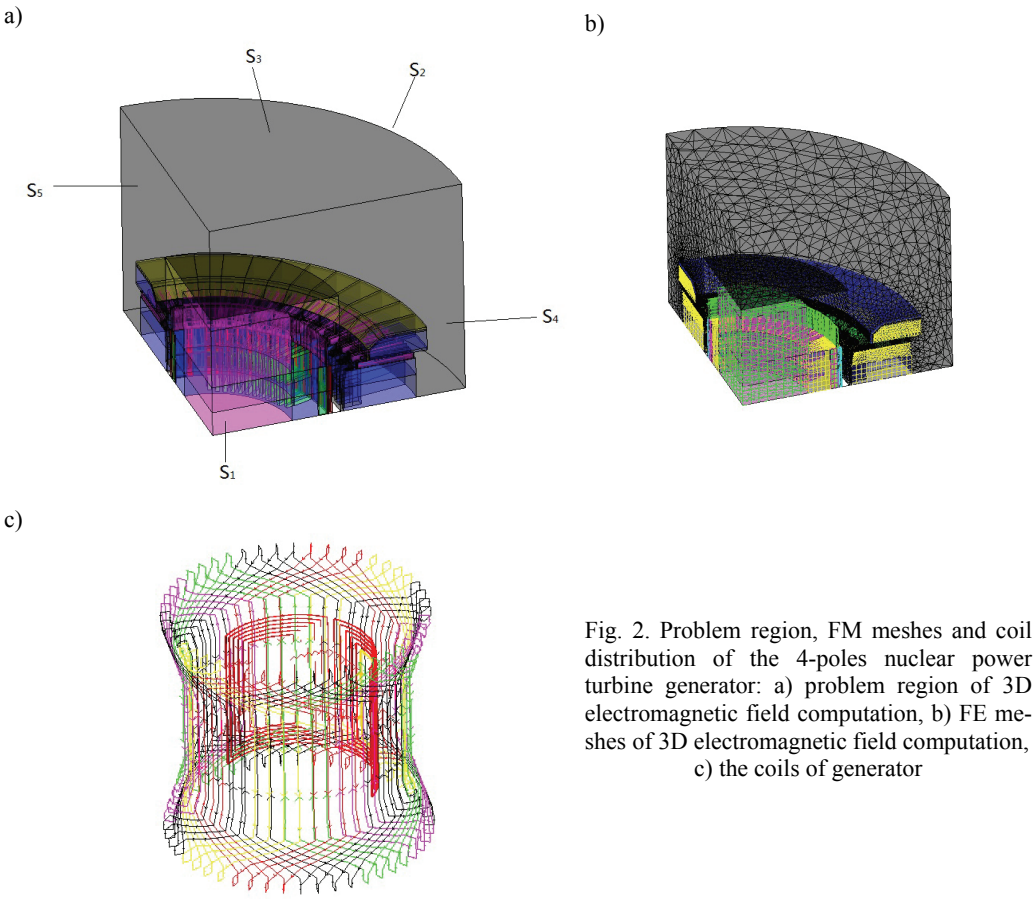

Fig. 2. Problem region, FM meshes and coil distribution of the 4-poles nuclear power turbine generator: a) problem region of 3D electromagnetic field computation, b) FE meshes of 3D electromagnetic field computation, c) the coils of generator

Considering the core saturation, by coulomb norm $\nabla \cdot \mathbf{A} = 0$ and the boundary condition of the problem region, the 3D boundary value problem of nonlinear time-varying moving electromagnetic field is then obtained:

$$\begin{aligned} &\nabla \times (\nu \nabla \times \mathbf{A}) + \sigma \left[\frac{\partial \mathbf{A}}{\partial t} - \mathbf{V} \times (\nabla \times \mathbf{A}) \right] = \mathbf{J}_S \\ &\left. \begin{aligned} &\mathbf{n} \times \mathbf{A} = 0 \\ &\frac{\partial A_n}{\partial n} = 0 \end{aligned} \right\} S_1, S_2, S_3 \\ &\mathbf{A}\big|_{S_4} = -\mathbf{A}\big|_{S_5}, \end{aligned} \tag{1}$$

where $\mathbf{A}$ is the magnetic vector potential, A_n is the normal component of $\mathbf{A}$, $\mathbf{J_s}$ is the source current density which is equal to $-\sigma \nabla \varphi$, ν is the reluctivity, $\mathbf{V}$ is the velocity, σ is the conductivity, S_1 is the symmetric boundary surface which is parallel with the flux line, S_2 is the

end shade, S_3 is the end cover idealized boundary with $\sigma = \infty$ on which contains only the tangential conponent of magnetic field, S_4 and S_5 are periodic boundary surfaces which are met the anticyclic boundary condition.

2.3. Application of the stator excitement

For the 3D electromagnetic field solving, the reasonable consideration of the stator current phasors is the key point of the stator winding excitement. Only if the phasors are accurate, can the operating state of the generator be simulated correctly.

The 2D field-circuit coupling model can set the operating states of the generator accurately, so it is used to determine the phasors of the stator 3-phase currents. The 2D FM meshes of problem region are shown in Figure 3.

In the 2D field-circuit coupling model, supposing the current density and magnetic vector potential have only the axial z components respectively, and the speed has only the tangential θ component, the 2D boundary value problem under the cylindrical coordinate is then obtained:

$$\begin{cases} \nu \dfrac{\partial^2 A_z}{\partial r^2} + \nu \dfrac{1}{r}\dfrac{\partial A_z}{\partial r} + \nu \dfrac{1}{r^2}\dfrac{\partial^2 A_z}{\partial \theta^2} = -J_z + \sigma \dfrac{\partial A_z}{\partial t} + V_\theta \sigma \dfrac{\partial A_z}{\partial \theta} \\ A_z\big|_{L_1} = 0 \\ A_z\big|_{L_2} = -A_z\big|_{L_3} \end{cases} . \tag{2}$$

Based on the stator coupling circuit shown in Figure 4, the voltage equations of the stator circuit are:

$$e_s = u_s + R_{1e} i_s + L_{1e} \frac{di_s}{dt}, \tag{3}$$

$$u_s = R_L i_s + L_L \frac{di_s}{dt}, \tag{4}$$

where e_s, u_s and i_s are the induced EMF, the voltage and the current of the stator phase winding respectively, R_{1e} and L_{1e} are the resistance and the leakage inductance of the stator end winding respectively, R_L and L_L are the resistance and inductance of loads respectively. Different operating states of the generator can be set by changing the value of R_L and L_L.

The coupling circuit equation and the electromagnetic equation are combined, the magnetic vector potential A_z can be calculated by the time-step FE method, and then the currents and their phasors can be obtained.

When the load resistance R_L and inductance L_L are infinite, the no-load operating state is simulated as shown in Figure 4. And the rated operating state is simulated when the R_L and L_L are the rated values, then the rated currents and their phasors are obtained, as shown in Figure 5.

The waveform and the stator current phasor at the different operating states are used as the excitement on the stator winding for the 3D FE analysis. And with the application of DC exciting current in the rotor field winding, 3D transient time-varying FE model can be solved.

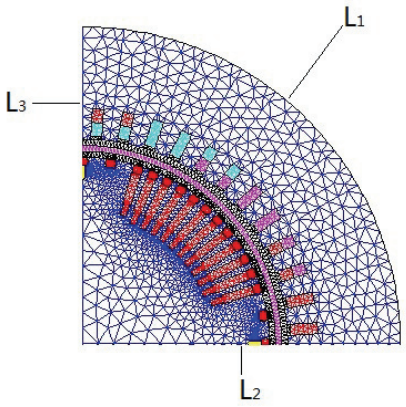

Fig. 3. 2D meshes for the computation of the stator current phasors

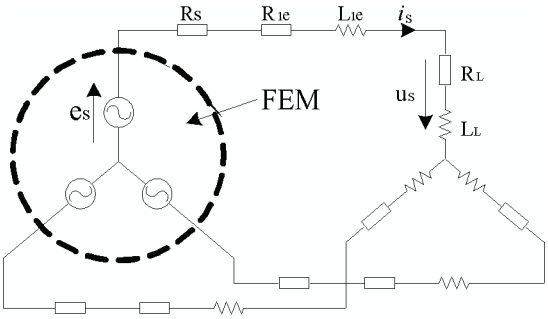

Fig. 4. The stator coupling circuit

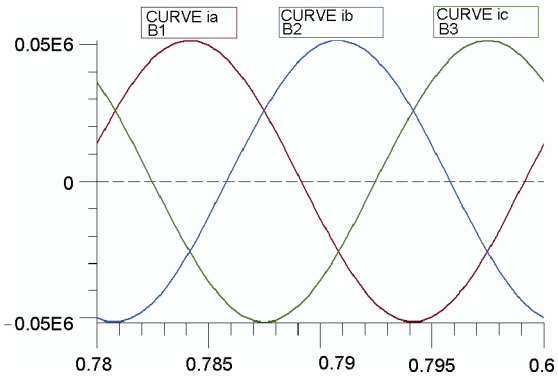

Fig. 5. The waveforms of stator currents at rated load

2.4. The eddy loss calculation of stator end region

According to the computation of 3D transient electromagnetic field, the instantaneous value of eddy current density and eddy loss density per element are obtained:

$$J = -\sigma \frac{\partial A}{\partial t}, \tag{5}$$

$$P_e = \frac{1}{\sigma}(J \cdot J). \tag{6}$$

And the average value of eddy loss density within a period is as follows:

$$P_{eav} = \frac{1}{T}\int_0^T p_e dt. \tag{7}$$

The average value of eddy loss in the volume is as follows:

$$P_{eddy} = \iiint_V dP_{eav}\, dv. \tag{8}$$

2.5. Treatment of the rotor motion

Because of the relative movement between the stator and the rotor, the FE meshes of the airgap will be distorted. If the rotor motion is handled inappropriately, the FE solution will be unstable, or even wrong.

So, in order to eliminate the velocity factor V from the electromagnetic field boundary value problem, the meshes of the stator and the rotor are separated, a slide layer including the airgap is used to couple the static stator and the rotating rotor. In the time-step FE analysis, when the rotor reaches to a new position, the elements of the slide layer will be rebuilt. The method will ensure the accuracy and convergence of FE computation.

2.6. Boundary value problem of 3D temperature field

The solving region for the 3D temperature field is the stator end region, including the magnetic shield, the clamping plate, the finger plate, the end ladder core, and so on.

The heat source is the eddy current loss and core loss calculated by the 3D transient electromagnetic field. Considering the anisotropic heat conduction condition of the laminated core, the boundary value problem of 3D steady temperature field can be expressed as follows:

$$\begin{cases} \dfrac{\partial}{\partial x}(\lambda_x \dfrac{\partial T}{\partial x}) + \dfrac{\partial}{\partial y}(\lambda_y \dfrac{\partial T}{\partial y}) + \dfrac{\partial}{\partial z}(\lambda_z \dfrac{\partial T}{\partial z}) = -q_V \\ \lambda \dfrac{\partial T}{\partial n}\Big|_S = -\alpha(T - T_f) \end{cases}, \tag{9}$$

where T is the temperature, λ_x, λ_y, λ_z are the coefficient of thermal conductivity on different directions which are shown in Table 2, q_v is the heat source density which is obtained by the loss calculation mentioned above, S are the surfaces of the stator end region related with the heat dissipation boundary condition, α is the heat transfer coefficient on S, T_f is the environment temperature which are shown in Table 3 at the different operating conditions.

Table 2. Coefficient of thermal conductivity of the stator end region components

Components	Coefficient of thermal conductivity (W/m · K)
Stator core	51 (X direction)
	51 (Ydirection)
	19.6 (Z direction)
Magnetic shield	375
Clamping plate	43
Finger plate	33
Insulating materials	0.16
The copper in stator bar	372

Table 3. Value of the environment temperature

Positions	T_f (°C)	
	No-load	Rated load
Stator bars cooling water pipe	33	52
The other part of stator end region	45	55

2.7. The confirmation of heat transfer coefficient

The heat generated from the stator end region is mainly carried away by convection. To confirm the heat transfer coefficient, the following assumptions are proposed based on meeting the practical engineering.

1) The surface of end region is smooth, and the fluid velocity on the same surface is constant.
2) Considering the end region is cooled by the forced convection and the heat radiation is ignorable.
3) Because there is no mechanical contact between the stator and the rotor, the influence of the rotor temperature rise is ignorable when the temperature field of the stator end region is calculated.

The heat transfer coefficient of the radial cooling duct is then as following [18, 19]:

$$\alpha_{rs} = K_{H_2} \cdot \frac{1+0.24w_{rs}}{0.045}. \tag{10}$$

The heat transfer coefficient of axial cooling duct is as following [18, 19]:

$$\alpha_{as} = K_{H_2} \cdot 44.9\left(\frac{30}{l}\right)^{0.256} \cdot r^{0.088} \cdot \left(\frac{w_{as}}{10}\right)^{0.832}, \tag{11}$$

$$K_{H_2} = 1.3\left(\frac{P}{P_0}\right)^{0.8}, \tag{12}$$

where w_{rs} and w_{as} are the average velocities of fluid in the radial and axial cooling ducts respectively, l is the length of the axial cooling duct, r is the hydraulic radius of the axial

cooling duct, P is the absolute pressure of Hydrogen, P_0 is the atmospheric pressure. The heat transfer coefficient of the stator tooth top surface is as following [18, 19].

$$\alpha_\delta = K_{H_2} \cdot 28(1+\sqrt{w_\delta}), \tag{13}$$

where w_δ is the average velocity of fluid in the airgap.

And the heat transfer coefficient of the cooling water pipe in the stator bars is as following [18, 19]:

$$\alpha_w = K_{H_2} \cdot (91.8) \cdot w^{0.8} (39.5 + T_w^{0.35}) \cdot d^{-0.2}, \tag{14}$$

where w is the average velocity of cooling water in the pipes, T_w is the average temperature of the water, and d is the hydraulic diameter of the cooling water pipe.

The heat transfer coefficients on the surfaces of other components in the stator end region, which come out of the above models, are as shown in Table 4.

Table 4. The heat transfer coefficients on the surfaces of some components in stator end region

Components	**Heat transfer coefficients (W/m^2 · K)**
Magnetic shield	615 ~ 1548
Clamping plate	765 ~ 1548
Finger plate	956
Radial cooling duct	1020
Cooling water pipe	15595 (rated load)
	15380 (no-load)

3. Computation results and discussions

3.1. The consideration of the key points for calculation and test

To validate the calculation, some key points at the end region of the generator are chosen. By installing the magnetic coil and the thermocouple, the magnetic density and the temperature at no-load and rated load are measured. The positions of key points are shown in Figure 6, in which A is at the low part of the magnetic shield, B is at the finger plate, C, D and E are at the tooth top of the 1st, the 2nd and the 3rd section of the end core teeth respectively.

3.2. Magnetic field and eddy current loss

Based on the models mention above, the magnetic field and the eddy current distribution are obtained, and then the loss and heat distribution are solved. Some of the results are shown in Figure 7 to Figure 11, and Table 5 to Table 7.

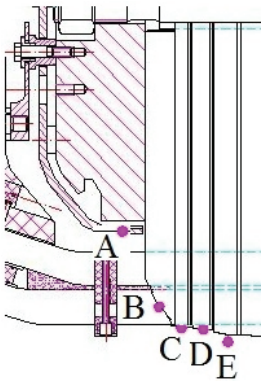

Fig. 6. Locations of measure points of the end region

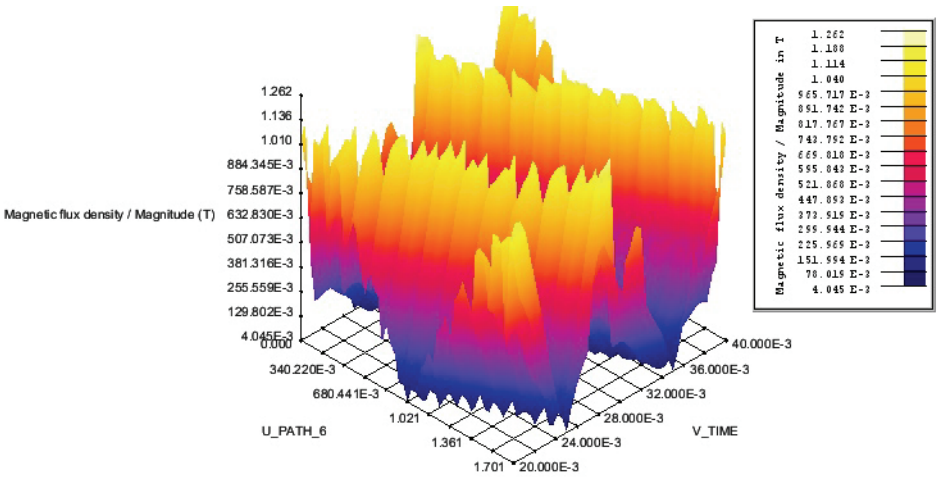

Fig. 7. The time-varying flux density including the key point A (no-load)

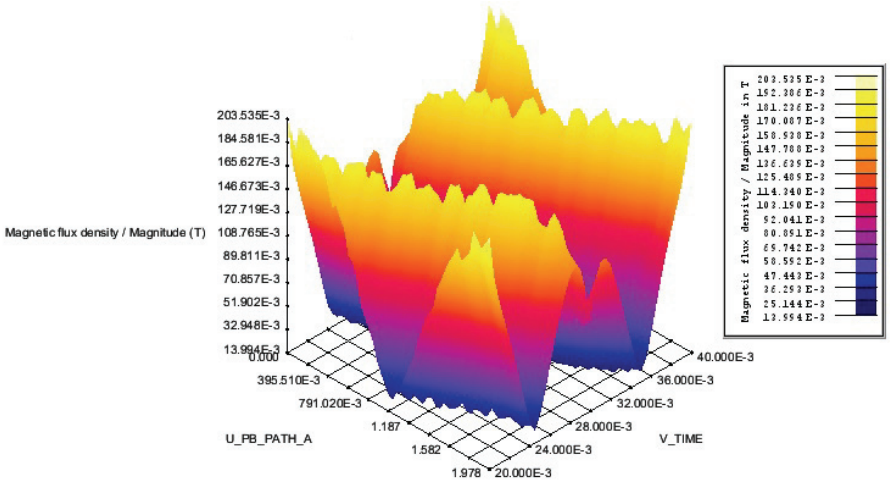

Fig. 8. The time-varying flux density including the key point C (no-load)

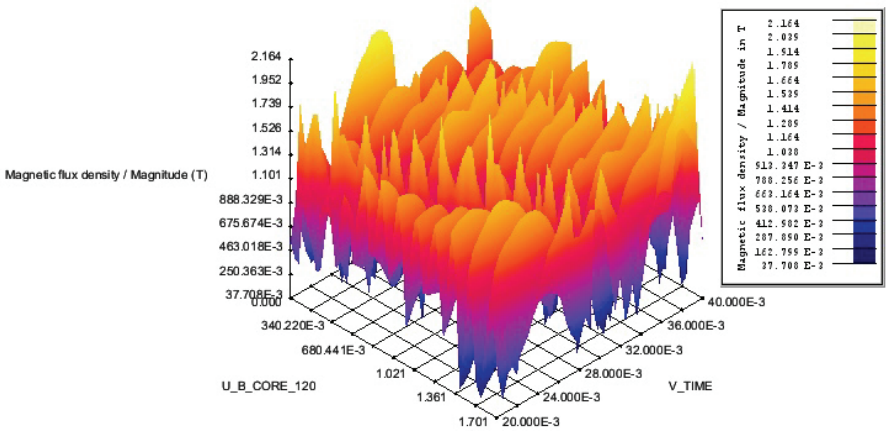

Fig. 9. The time-varying flux density including the key point A (rated load)

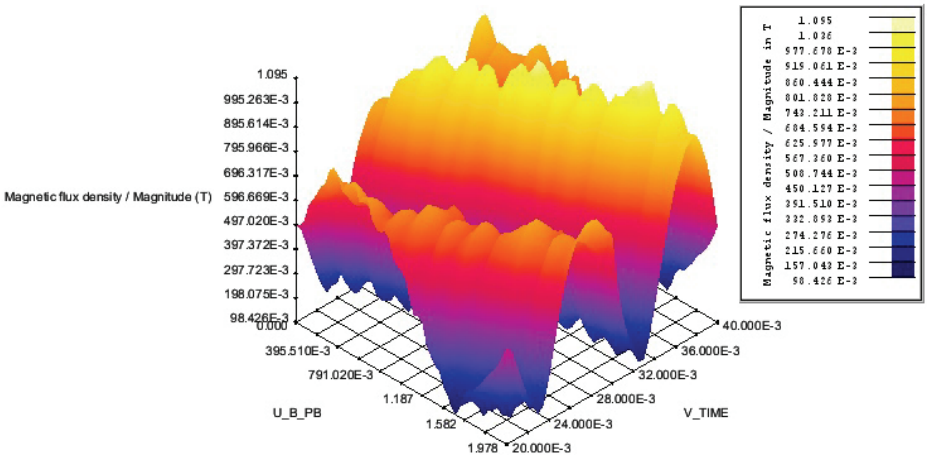

Fig. 10. The time-varying flux density including the key point C (rated load)

Table 5. Eddy loss of the region components

Components	No-load (kW)	Rated load (kW)
Magnetic shield	22.78	69.09
Clamping plate	22.22	36.77
Finger plate	53.33	70.29

From Figure 7 to Figure11, the time varying magnetic flux density of the points A and C at no-load and rated load are shown. It can be seen that the magnetic flux density at each circle is changing over time, and the waveforms are roughly similar.

(a) $t = 0.005$ s

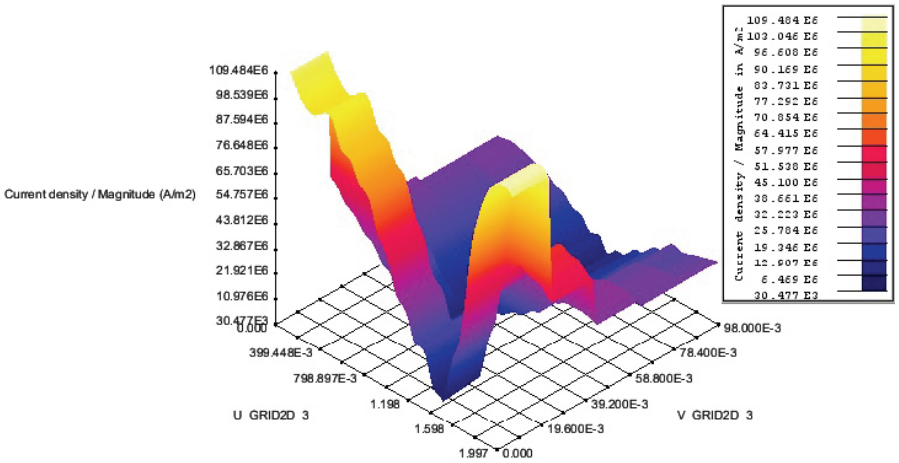

(b) $t = 0.035$ s

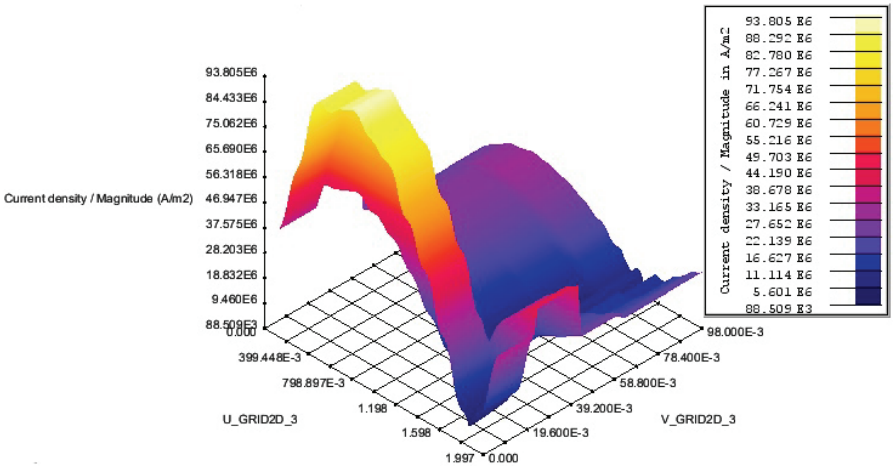

Fig. 11. Eddy density including the key point A at different time (rated load)

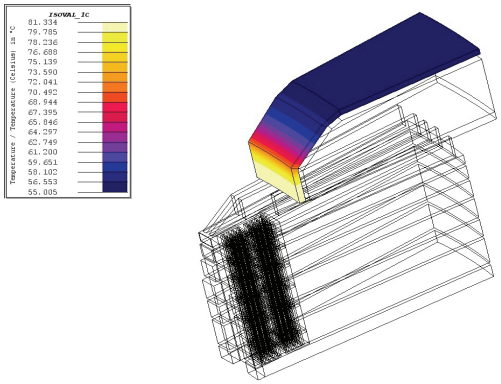

Fig. 12. Temperature distribution of the magnetic shield at rated load (the stator bars are included in the temperature field solving region)

Table 6. Max temperature of the end region components

Components	With stator bars (°C)		Without stator bars (°C)	
	no-load	rated load	no-load	rated load
Magnetic shield	53.68	81.33	53.68	81.33
Clamping plate	50.61	64.04	50.61	64.19
Finger plate	49.30	61.03	49.31	61.37
1st section of end core teeth	46.94	59.66	47.05	59.98
2nd section of end core teeth	48.35	64.02	48.67	64.76
3rd section of end core teeth	47.03	60.57	47.39	61.34

Figure11 shows the change of eddy current with time of the low part of magnetic shield which includes the point A. It can be seen that, although the eddy current density at each point on the magnetic shield is varying with time, the maximum eddy current density at the area is close to the core lamination.

Table 5 shows that the eddy current loss is concentrated in the magnetic shield and the finger plate, no matter at no-load or at rated load. Since the maximum eddy current density is focused at the low part of the magnetic shield and the finger plate, the maximum eddy current loss density is focused at the same area. Because the material in the area is conductor, and it is very near the windings, the induced eddy current losses are much larger than those of other area. And the close space of the low part of the magnetic shield is limited and the cooling condition is difficult, so the maximum temperature at the end region is focused at this area, as shown in Figure12 and Table 6.

In addition, by the data comparison of Table 6, the highest temperature is hardly changed between the models with or without considering the heat of stator bars. The reason is that, the thermal property of slot insulation material is well and the heat dissipation capacity of cooling water inside the stator bars is strong, so the heat of stator bars is difficult to affect the rest area of end region. Then, the heat effect of stator bars can be neglected in the calculation.

3.3. Verification of the results

To verify the correctness of the models and the calculated results, the magnetic flux density at no-load and the temperature at no-load and rated load are measured. The calculated results and the test data are shown in Tables 7-9.

Table 7. Flux density of the end region components at no-load

Key points	Magnetic flux density (T)		
	computed	measured	relative error [%]
A	0.11	0.12	8.3
B	0.25	0.27	7.4
C	0.70	0.76	7.9
D	0.69	0.73	5.5
E	0.77	0.79	2.5
The average error			6.32

Table 8. Temperature of the end region components at no-load (consider the stator bars)

Key points	**Temperature (°C)**		
	computed	measured	relative error [%]
A	53.68	51.37	4.5
B	49.30	43.01	14.6
C	46.94	48.05	2.3
D	48.35	51.55	6.2
E	47.03	45.08	4.3
The average error			6.38

Table 9. Temperature of the end region components at rated load (consider the stator bars)

Key points	**Temperature (°C)**		
	computed	measured	relative error [%]
A	81.33	91.26	10.9
B	61.03	58.93	3.6
C	59.66	64.75	7.9
D	64.02	66.46	3.4
E	60.57	58.60	3.4
The average error			5.84

The comparison shows that the calculated results are well coincident with the test data.

4. Conclusions

In this paper, a 50 Hz, 1150 MW, 4-poles nuclear power turbine generator operating at no-load and rated load are analyzed by the 3D transient electromagnetic field and 3D steady temperature field, the loss and heat at the end region are calculated. Compared with the 2D axis symmetric models, quasi-3D models, 3D static magnetic models and 3D steady AC magnetic, the models of this paper consider more factors such as the structure, the material, the eddy current, the rotor motion, the complexity of conductivity and heat-sinking capability. Then the distribution of loss and heat at the generator end region are obtained the calculated results are well coincident with the measured data. The research is helpful to enhance the design standard of large 4-poles nuclear power turbine generator, and has been applied in the design and manufacture of the 1550 MW and 1760 MW 4-poles nuclear power turbine generators.

Acknowledgements
This work was sponsored by the Chinese National Key Special Research Sub-project. Project No. 2010ZX06004-013-04-02.

References

[1] Hrioshi O., *Calculation of the magnetic field in the end region of a generator*. Proc. Electr. Soc. 89(10), (1969).

[2] Kaoru Ito, Tadashi Tokumasu, Susumu Nagamo et al, *Simulation for design purposes of magnetic fields in turbine-driven generator end region.* IEEE Transactions on Power Apparatuss and Systems 99(4): 1586-1596 (1980).

[3] Weise J., Stephens C.M., *Finite Elements for Three-Dimensional Magnetostatic Fields and its Application to Turbine-Generator End Regions.* IEEE Transactions on Power Apparatus and Systems 100(4): 1591-1596 (1981).

[4] Khan M.G.K., Buckley G.W., Bennett R.B. et al, *An integrated approach for the calculation of losses and temperature in the end-region of large turbine generators*. IEEE Transactions on Energy Conversion 5(1):183-194 (1990).

[5] Plantive E., Salon S., Chair M.V.K., *Advances in the axiperiodic magnetostatic analysis of generator end regions*. IEEE Transactions on Mganetics 32(5): 4278-4290 (1996).

[6] Tang Renyuan, Xu Guangren, Tian Lijian, Zhao Danqun, *Calculation of end region magnetic field and circulating losses for turbo-generator using a coupled field and circuit equation method*. IEEE Transactions on Mganetics 26(2): 497-500 (1990).

[7] Huang Xueliang, Hu Minqiang, Du Yansen, Zhou E, *Research on the eddy current electromagnetic field in the end region of turbogenerator and which affect the field*, Transactions of China Electrotechnical Society 15(6) 1-4 (2000).

[8] Drago Ban, Zarko D., Mandi I., *Turbogenerator end winding leakage inductance calculation using a 3-D analytical approach based on the solution of Neuman integrals*. IEEE Transactions on Energy Conversion 20(1): 98-105 (2005).

[9] Li Jinxiang, Sun Yutian, Yang Guijie, *Calculation and analysis of 3D magnetic field for end region of large turbogenerators.* International Conference on Electrical Machines and Systems 2005, ICEMS pp. 2079-2082 (2005).

[10] Masafumi Fujita, Tadashi Tokumasu, Hiroyuki Yoda et al., *Magnetic field analysis of stator core end region of large turbogenerators.* IEEE Transactions on magnetics 36(4): 1850-1853 (2000).

[11] Yingying Yao, Haixia Xia, Guangzheng Ni et al, *3-D eddy current analysis in the end region of a turbogenerator by using reduced magnetic vector potential.* IEEE Transactions on magnetics 42(4): 1323-1326 (2006).

[12] Masafumi Fujita, Tadashi Ueda, Tadashi Tokumasu et al., *Eddy current analysis in the stator end structures of large capacity turbine generators.* International Conference on Electrical Machines and Systems 2009, ICEMS, pp. 1-6 (2009).

[13] Du Yansen, Huang Xueliang, Liu Lei, Hu Minqiang, *Study on temperature distribution in the end region of large turbogenerator*. Proceedings of CSEE 16(2): 95-101 (1996).

[14] Lu Diqiang, Huang Xueliang, Hu Minqiang, *Using finite element method to calculate 3D thermal distribution in the end region of turbo-generator.* Proceedings of CSEE 21(3): 81-85 (2001).

[15] Xia Hai-xia, Yao Ying-ying, Xiong Su-ming et al., *Magnetic-thermal coupling analysis of end region of 1000 MW turbine-generator.* Proceedings of CSEE 28(14): 118-122 (2008).

[16] Li Wei-li, Li Yong,Yang Xue-feng et al, *Temperature and fluid flow field calculation an analysis of stator end of air cooled turbo-generator*. Proceedings of CSEE 29(36): 80-87 (2009).

[17] Li Wei-li, Guang Chunwei, Zheng Ping, *Calculation of a Complex 3-D Model of a Turbogenerator With End Region Regarding Electrical Losses,Cooling ,and Heating.* IEEE Transactions on Energy Conversion 26(4): 1073-1080 (2010).

[18] Yong-Tian Wei Da-Wei Meng, Jia-Bin Wen, *Heat Exchange in Electrical Machine.* Beijing: China Machine Press (1998).

[19] Sun-nian Ding, *The Heating and Cooling of Large Electrical Machine.* Beijing: China Science Press (1991).